

## **Finite Element Transient Dynamic Analysis of Isotropic and Fibre Reinforced Composite Plates Using a Higher-order Theory**

T. Kant, R. V. Ravichandran, B. N. Pandya and Mallikarjuna

Department of Civil Engineering, Indian Institute of Technology, Powai,  
Bombay 400 076, India

### *ABSTRACT*

*A higher-order shear deformable  $C^0$  continuous finite element is developed and employed to investigate the transient response of isotropic, orthotropic and layered anisotropic composite plates. The governing ordinary linear differential equations are integrated using the central difference explicit time integration scheme. A special mass matrix diagonalization scheme is adopted which conserves the total mass of the element and includes the effects due to rotary inertia terms. Numerical results for deflections and stresses are presented for rectangular plates under various boundary conditions and loadings. The parametric effects of the time step, finite element mesh, lamination scheme and orthotropy on the transient response are investigated. The numerical results are compared with those available in the literature, and with the results obtained by solving the same problems using the Mindlin plate element.*

### 1 INTRODUCTION

The classical laminate theory based on Kirchhoff's hypothesis<sup>1,2</sup> was the starting point in the analysis of laminated plates. This theory ignores the effects of transverse shear strains and the normal strain in the thickness direction. These effects are pronounced in laminated composite plates owing to a very high ratio of inplane elastic modulus to transverse shear modulus (of the order of 25–40). Further it was also noted that the classical plate theory is computationally inefficient from the point of view of simple finite element formulation.<sup>3</sup>

Reissner<sup>4</sup> and Mindlin<sup>5</sup> are the first ones to provide first-order shear deformation theories. Both these theories yield a  $C^0$  continuous finite element formulation for the numerical analysis but have certain limitations: the transverse shear stress/strains are assumed constant through the plate thickness and a fictitious shear correction coefficient is introduced; the classical contradiction whereby both the transverse normal stress and the transverse normal strain are neglected remains unresolved.

Theories based on realistic displacement models which give rise to nonlinear distribution of inplane normal strains and transverse shear strains have been developed by Murthy,<sup>6</sup> and Phan and Reddy.<sup>7</sup> Lo *et al.*<sup>8,9</sup> and Kant<sup>10</sup> have, in addition, included the effects of transverse normal strain and stress in their theories. Kant *et al.*<sup>11</sup> have presented a  $C^0$  finite element formulation of the higher-order theory. Pandya and Kant<sup>12</sup> have extended the above formulation for generally orthotropic plates.

The linear elastic transient response of plates has been studied by Reismann<sup>13</sup> and Lee and Reismann<sup>14</sup> using three dimensional elasticity, classical and improved plate theories. Rock and Hinton,<sup>15</sup> Hinton<sup>16</sup> and Pica and Hinton<sup>17,18</sup> have investigated the transient response of isotropic plates based on Reissner–Mindlin thick plate theory. Forced motions and transient response of rectangular composite plates have been studied by Reddy.<sup>19,20</sup> Here the Newmark's direct-integration is employed to numerically integrate the governing differential equation.

All the work so far reported on the transient response of plates is confined to either CPT or a first-order shear deformable theory. In the present work, a higher-order displacement field-based  $C^0$  finite element is used to study the transient response of isotropic and layered anisotropic plates for various loading and boundary conditions. The governing dynamic differential equations are integrated using the central difference explicit time integration scheme. The effects of coupling on the transient response are also investigated.

## 2 THEORY AND FORMULATION

The development of the present higher-order theory starts with the assumption of the displacement field in the following form:

$$\begin{aligned}
 U(x, y, z, t) &= u(x, y, t) + z\theta_x(x, y, t) + z^2 u^*(x, y, t) + z^3 \theta_x^*(x, y, t) \\
 V(x, y, z, t) &= v(x, y, t) + z\theta_y(x, y, t) + z^2 v^*(x, y, t) + z^3 \theta_y^*(x, y, t) \\
 W(x, y, z, t) &= w(x, y, t) + z\theta_z(x, y, t) + z^2 w^*(x, y, t)
 \end{aligned} \tag{1}$$

where:  $t$  is the time;  $U, V, W$  are the displacements of a general point in the  $x, y, z$  directions respectively;  $u, v, w$  are the associated midplane displacements;  $\theta_x$  and  $\theta_y$  are the slopes in the  $xz$  and  $yz$  directions due to bending only and  $u^*, v^*, w^*, \theta_x^*, \theta_y^*$  and  $\theta_z$  are the corresponding higher-order terms in the Taylor series expansion and are defined at the reference plane. The positive directions are shown in Fig. 1.

By substitution of these relations in the strain–displacement equations of the classical theory of elasticity,<sup>1</sup> the following relationships are obtained.

$$\begin{aligned}\epsilon_x^z &= \epsilon_x + zK_x + z^2\epsilon_x^* + z^3K_x^* \\ \epsilon_y^z &= \epsilon_y + zK_y + z^2\epsilon_y^* + z^3K_y^* \\ \epsilon_z^z &= \epsilon_z + zK_z \\ \gamma_{xy}^z &= \epsilon_{xy} + zK_{xy} + z^2\epsilon_{xy}^* + z^3K_{xy}^* \\ \gamma_{yz}^z &= \epsilon_{yz} + zK_{yz} + z^2\epsilon_{yz}^* \\ \gamma_{xz}^z &= \epsilon_{xz} + zK_{xz} + z^2\epsilon_{xz}^*\end{aligned}\quad (2a)$$

in which

$$\begin{aligned}\{\epsilon_x, \epsilon_y, \epsilon_z, \epsilon_{xy}\}^T &= \left\{ \frac{\partial u}{\partial x}, \frac{\partial v}{\partial y}, \theta_z, \frac{\partial u}{\partial y} + \frac{\partial v}{\partial x} \right\}^T \\ \{\epsilon_x^*, \epsilon_y^*, \epsilon_{xy}^*\}^T &= \left\{ \frac{\partial u^*}{\partial x}, \frac{\partial v^*}{\partial y}, \frac{\partial u^*}{\partial y} + \frac{\partial v^*}{\partial x} \right\}^T \\ \{K_x, K_y, K_z, K_{xy}\}^T &= \left\{ \frac{\partial \theta_x}{\partial x}, \frac{\partial \theta_y}{\partial y}, 2w^*, \frac{\partial \theta_x}{\partial y} + \frac{\partial \theta_y}{\partial x} \right\}^T \\ \{K_x^*, K_y^*, K_{xy}^*\}^T &= \left\{ \frac{\partial \theta_x^*}{\partial x}, \frac{\partial \theta_y^*}{\partial y}, \frac{\partial \theta_x^*}{\partial y} + \frac{\partial \theta_y^*}{\partial x} \right\}^T \\ \{\epsilon_{yz}, \epsilon_{xz}\}^T &= \left\{ \frac{\partial w}{\partial y} + \theta_y, \frac{\partial w}{\partial x} + \theta_x \right\}^T \\ \{K_{yz}, K_{xz}\}^T &= \left\{ 2v^* + \frac{\partial \theta_z}{\partial y}, 2u^* + \frac{\partial \theta_z}{\partial x} \right\}^T \\ \{\epsilon_{yz}^*, \epsilon_{xz}^*\}^T &= \left\{ 3\theta_y^* + \frac{\partial w^*}{\partial y}, 3\theta_x^* + \frac{\partial w^*}{\partial x} \right\}^T\end{aligned}\quad (2b)$$

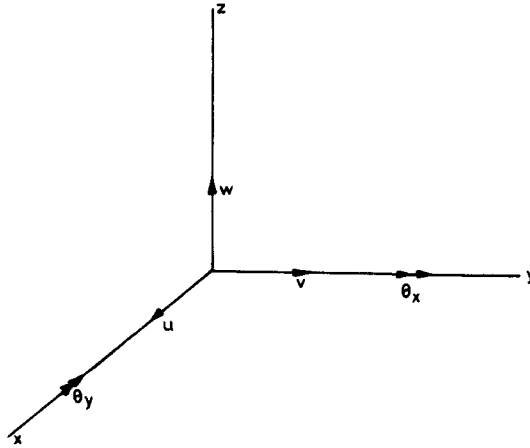


Fig. 1. Positive set of displacement components.

The stress–strain relationship for the  $L^{\text{th}}$  (layer) lamina of the composite laminate has the following form:

$$\begin{Bmatrix} \sigma_x \\ \sigma_y \\ \sigma_z \\ \tau_{xy} \\ \tau_{yz} \\ \tau_{xz} \end{Bmatrix} = \begin{bmatrix} Q_{11} & Q_{12} & Q_{13} & Q_{14} & 0 & 0 \\ Q_{12} & Q_{22} & Q_{23} & Q_{24} & 0 & 0 \\ Q_{13} & Q_{23} & Q_{33} & Q_{34} & 0 & 0 \\ Q_{14} & Q_{24} & Q_{34} & Q_{44} & 0 & 0 \\ 0 & 0 & 0 & 0 & Q_{55} & Q_{56} \\ 0 & 0 & 0 & 0 & Q_{56} & Q_{66} \end{bmatrix} \begin{Bmatrix} \epsilon_x \\ \epsilon_y \\ \epsilon_z \\ \gamma_{xy} \\ \gamma_{yz} \\ \gamma_{xz} \end{Bmatrix} \tag{3a}$$

This may be written in a compact form as

$$\boldsymbol{\sigma} = \mathbf{Q}\boldsymbol{\epsilon} \tag{3b}$$

where  $\boldsymbol{\sigma}$  and  $\boldsymbol{\epsilon}$  are the stress and strain vectors respectively with reference to the plate axes  $(x, y, z)$  (see Fig. 2). The stiffness matrix  $\mathbf{Q}$  with reference to plate axes is obtained from the stiffness matrix  $\mathbf{C}$  with reference to fibre axes (1-2-3) by using the coordinate transformation  $\mathbf{T}$  from the relation<sup>12</sup>

$$\mathbf{Q} = \mathbf{T}^{-1}\mathbf{C}[\mathbf{T}^{-1}]^T \quad \text{with} \quad \boldsymbol{\sigma}_{1-2-3} = \mathbf{T}\boldsymbol{\sigma}_{x-y-z} \tag{4}$$

Integration of eqns (3) through the plate thickness with strain terms given by eqns (2) gives the plate constitutive relations. The constitutive relations involving membrane forces are given by

$$\mathbf{N} = \mathbf{D}_m\boldsymbol{\epsilon}_m + \mathbf{D}_c\mathbf{K} \tag{5a}$$

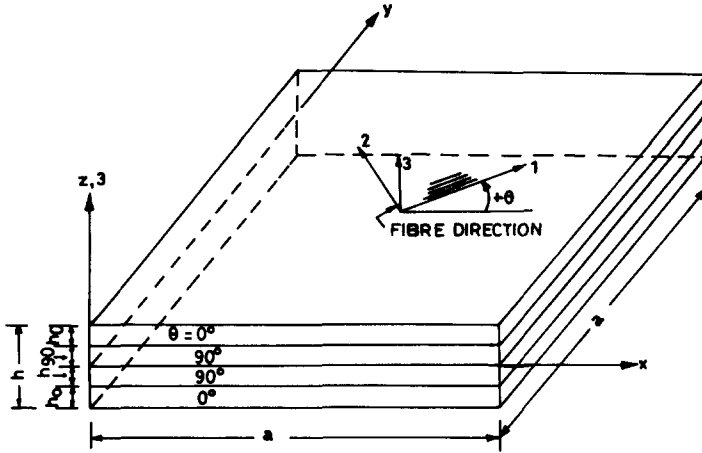


Fig. 2. Plate and fibre axes.

in which

$$\mathbf{N} = \{N_x, N_y, N_{xy}, N_x^*, N_y^*, N_{xy}^*, N_z\}^T$$

$$\boldsymbol{\epsilon}_m = \{\epsilon_x, \epsilon_y, \epsilon_{xy}, \epsilon_x^*, \epsilon_y^*, \epsilon_{xy}^*, \epsilon_z\}^T$$

$$\mathbf{K} = \{K_x, K_y, K_{xy}, K_x^*, K_y^*, K_{xy}^*, K_z\}^T$$

$$\mathbf{D}_m = \sum_{L=1}^n \begin{bmatrix} Q_{11}H_1 & Q_{12}H_1 & Q_{14}H_1 & Q_{11}H_3 & Q_{12}H_3 & Q_{14}H_3 & Q_{13}H_1 \\ & Q_{22}H_1 & Q_{24}H_1 & Q_{12}H_3 & Q_{22}H_3 & Q_{24}H_3 & Q_{23}H_1 \\ & & Q_{44}H_1 & Q_{14}H_3 & Q_{24}H_3 & Q_{44}H_3 & Q_{34}H_1 \\ & & & Q_{11}H_5 & Q_{12}H_5 & Q_{14}H_5 & Q_{13}H_3 \\ & & & & Q_{22}H_5 & Q_{24}H_5 & Q_{22}H_3 \\ & & & & & Q_{44}H_5 & Q_{34}H_3 \\ \text{Symmetric} & & & & & & Q_{33}H_1 \end{bmatrix} L^{\text{th}} \text{ layer} \quad (5b)$$

$$\mathbf{D}_c = \sum_{L=1}^n \begin{bmatrix} Q_{11}H_2 & Q_{12}H_2 & Q_{14}H_2 & Q_{11}H_4 & Q_{12}H_4 & Q_{14}H_4 & Q_{13}H_2 \\ & Q_{22}H_2 & Q_{24}H_2 & Q_{12}H_4 & Q_{22}H_4 & Q_{24}H_4 & Q_{23}H_2 \\ & & Q_{44}H_2 & Q_{14}H_4 & Q_{24}H_4 & Q_{44}H_4 & Q_{34}H_2 \\ & & & Q_{11}H_6 & Q_{12}H_6 & Q_{14}H_6 & Q_{13}H_4 \\ & & & & Q_{22}H_6 & Q_{24}H_6 & Q_{23}H_4 \\ & & & & & Q_{44}H_6 & Q_{34}H_4 \\ \text{Symmetric} & & & & & & Q_{33}H_2 \end{bmatrix} L^{\text{th}} \text{ layer} \quad (5c)$$

The elements of the membrane force vector  $\mathbf{N}$  are defined as follows:

$$\begin{Bmatrix} N_x, N_x^* \\ N_y, N_y^* \\ N_{xy}, N_{xy}^* \end{Bmatrix} = \sum_{L=1}^n \int_{h_{L+1}}^{h_L} \begin{Bmatrix} \sigma_x \\ \sigma_y \\ \tau_{xy} \end{Bmatrix} [1, z^2] dz \quad (5d)$$

$$N_z = \sum_{L=1}^n \int_{h_{L+1}}^{h_L} \sigma_z dz \quad (5e)$$

The constitutive relations involving bending moments are given by

$$\mathbf{M} = \mathbf{D}_c \boldsymbol{\epsilon}_m + \mathbf{D}_b \mathbf{K} \quad (6a)$$

where

$$\mathbf{M} = \{M_x, M_y, M_{xy}, M_x^*, M_y^*, M_{xy}^*, M_z\}^T$$

$$\mathbf{D}_b = \sum_{L=1}^n \begin{bmatrix} Q_{11}H_3 & Q_{12}H_3 & Q_{14}H_3 & Q_{11}H_5 & Q_{12}H_5 & Q_{14}H_5 & Q_{13}H_3 \\ & Q_{22}H_3 & Q_{24}H_3 & Q_{12}H_5 & Q_{22}H_5 & Q_{24}H_5 & Q_{23}H_3 \\ & & Q_{44}H_3 & Q_{14}H_5 & Q_{24}H_5 & Q_{44}H_5 & Q_{34}H_3 \\ & & & Q_{11}H_7 & Q_{12}H_7 & Q_{14}H_7 & Q_{13}H_5 \end{bmatrix} L^{\text{th}} \text{ layer}$$

The constitutive relations involving shear forces are given by

$$\mathbf{Q} = \mathbf{D}_s \Phi \tag{7a}$$

where

$$\mathbf{Q} = \{S_x, S_y, Q_x, Q_y, Q_x^*, Q_y^*\}^T$$

$$\Phi = \{K_{xz}, K_{yz}, \epsilon_{xz}, \epsilon_{yz}, \epsilon_{xz}^*, \epsilon_{yz}^*\}^T$$

$$\mathbf{D}_s = \sum_{L=1}^n \begin{bmatrix} Q_{66}H_3 & Q_{56}H_3 & Q_{66}H_2 & Q_{56}H_2 & Q_{66}H_4 & Q_{56}H_4 \\ & Q_{55}H_3 & Q_{56}H_2 & Q_{55}H_2 & Q_{56}H_4 & Q_{55}H_4 \\ & & Q_{66}H_1 & Q_{56}H_1 & Q_{66}H_3 & Q_{56}H_3 \\ & & & Q_{55}H_1 & Q_{56}H_3 & Q_{55}H_3 \\ & & & & Q_{66}H_5 & Q_{56}H_5 \\ \text{Symmetric} & & & & & Q_{55}H_5 \end{bmatrix} L^{\text{th}} \text{ layer} \tag{7b}$$

The components of the shear force vector are given by

$$\begin{pmatrix} Q_x, S_x, Q_x^* \\ Q_y, S_y, Q_y^* \end{pmatrix} = \sum_{L=1}^n \int_{h_{L+1}}^{h_L} \begin{pmatrix} \tau_{xz} \\ \tau_{yz} \end{pmatrix} [1, z, z^2] dz \tag{7c}$$

In all the above relations,  $n$  is the number of layers and

$$H_i = \frac{l}{i}(h_L^i - h_{L+1}^i) ; i = 1, 2, \dots, 7$$

### 3 FINITE ELEMENT DISCRETIZATION

Finite element spatial discretization schemes, when applied to dynamic transient structural analysis problems, result in a set of ordinary differential equations. In the absence of damping these equations take the form

$$\mathbf{M}\ddot{\mathbf{a}} + \mathbf{K}\mathbf{a} = \mathbf{P}(t) \tag{8}$$

in which the dots define differentiation with time  $t$ ,  $\mathbf{a}$  is the nodal displacement vector,  $\mathbf{M}$  is the mass matrix and  $\mathbf{P}$  is the vector of forces which varies with time,  $t$ .

The generalized displacement of the reference plane is expressed in terms of eleven independent variables as:

$$\mathbf{a} = \{u, v, w, \theta_x, \theta_y, \theta_z, u^*, v^*, w^*, \theta_x^*, \theta_y^*\}^T \quad (9)$$

In  $C^0$  finite element theory, the continuum displacement vector within the element is discretized such that

$$\mathbf{a} = \sum_{i=1}^{NE} N_i(x, y) \mathbf{a}_i \quad (10)$$

in which the term  $N_i(x, y)$  is the interpolating or shape function associated with node  $i$ ,  $\mathbf{a}_i$  is the value of  $\mathbf{a}$  corresponding to node  $i$  and  $NE$  is the number of nodes in the elements. Equation (10) ensures that the approximate  $\mathbf{a}$  is not only continuous within the element but over the entire domain since the same value of  $\mathbf{a}$  is used for all the elements at the common nodes.

With the generalized displacement vector  $\mathbf{a}$  known at all points within the element as per eqn (9), the generalized strain vector  $\boldsymbol{\epsilon}$  at any point is expressed as follows:

$$\begin{bmatrix} \frac{\partial N_i}{\partial x} & 0 & 0 & 0 & 0 & 0 & 0 & 0 & 0 & 0 & 0 \\ 0 & \frac{\partial N_i}{\partial y} & 0 & 0 & 0 & 0 & 0 & 0 & 0 & 0 & 0 \\ \frac{\partial N_i}{\partial y} & \frac{\partial N_i}{\partial x} & 0 & 0 & 0 & 0 & 0 & 0 & 0 & 0 & 0 \\ 0 & 0 & 0 & 0 & 0 & 0 & \frac{\partial N_i}{\partial x} & 0 & 0 & 0 & 0 \\ 0 & 0 & 0 & 0 & 0 & 0 & 0 & \frac{\partial N_i}{\partial y} & 0 & 0 & 0 \\ 0 & 0 & 0 & 0 & 0 & 0 & \frac{\partial N_i}{\partial y} & \frac{\partial N_i}{\partial x} & 0 & 0 & 0 \\ 0 & 0 & 0 & 0 & 0 & N_i & 0 & 0 & 0 & 0 & 0 \\ 0 & 0 & 0 & \frac{\partial N_i}{\partial x} & 0 & 0 & 0 & 0 & 0 & 0 & 0 \\ 0 & 0 & 0 & 0 & \frac{\partial N_i}{\partial y} & 0 & 0 & 0 & 0 & 0 & 0 \end{bmatrix} \begin{bmatrix} u_i \\ v_i \\ w_i \\ \theta_{xi} \\ \theta_{yi} \end{bmatrix}$$

$$\boldsymbol{\epsilon} = \sum_{i=1}^{NE} \begin{bmatrix}
 0 & 0 & 0 & \frac{\partial N_i}{\partial y} & \frac{\partial N_i}{\partial x} & 0 & 0 & 0 & 0 & 0 & 0 \\
 0 & 0 & 0 & 0 & 0 & 0 & 0 & 0 & 0 & \frac{\partial N_i}{\partial x} & 0 \\
 0 & 0 & 0 & 0 & 0 & 0 & 0 & 0 & 0 & 0 & \frac{\partial N_i}{\partial y} \\
 0 & 0 & 0 & 0 & 0 & 0 & 0 & 0 & 0 & \frac{\partial N_i}{\partial y} & \frac{\partial N_i}{\partial x} \\
 0 & 0 & 0 & 0 & 0 & 0 & 0 & 0 & 2N_i & 0 & 0 \\
 0 & 0 & 0 & 0 & 0 & \frac{\partial N_i}{\partial x} & 2N_i & 0 & 0 & 0 & 0 \\
 0 & 0 & 0 & 0 & 0 & \frac{\partial N_i}{\partial y} & 0 & 2N_i & 0 & 0 & 0 \\
 0 & 0 & \frac{\partial N_i}{\partial x} & N_i & 0 & 0 & 0 & 0 & 0 & 0 & 0 \\
 0 & 0 & \frac{\partial N_i}{\partial y} & 0 & N_i & 0 & 0 & 0 & 0 & 0 & 0 \\
 0 & 0 & 0 & 0 & 0 & 0 & 0 & 0 & \frac{\partial N_i}{\partial x} & 3N_i & 0 \\
 0 & 0 & 0 & 0 & 0 & 0 & 0 & 0 & \frac{\partial N_i}{\partial y} & 0 & 3N_i
 \end{bmatrix} \begin{Bmatrix}
 \theta_{zi} \\
 u_i^* \\
 v_i^* \\
 w_i^* \\
 \theta_{xi}^* \\
 \theta_{yi}^* \\
 \\
 \\
 \\
 \\
 \\
 \end{Bmatrix} \tag{11a}$$

or

$$\boldsymbol{\epsilon} = \sum_{i=1}^{NE} \mathbf{B}_i \mathbf{a}_i \tag{11b}$$

where

$$\boldsymbol{\epsilon} = \{ \epsilon_x, \epsilon_y, \epsilon_{xy}, \epsilon_x^*, \epsilon_y^*, \epsilon_{xy}^*, \epsilon_z, K_x, K_y, K_{xy}, K_x^*, K_y^*, K_{xy}^*, K_z, K_{xz}, K_{yz}, \epsilon_{xz}, \epsilon_{yz}, \epsilon_{xz}^*, \epsilon_{yz}^* \}^T \tag{11c}$$

The elasticity matrix **D** is obtained by combining eqns (5)–(7) as follows:

$$\mathbf{D} = \begin{bmatrix}
 \mathbf{D}_m & \mathbf{D}_c & 0 \\
 \mathbf{D}_c & \mathbf{D}_b & 0 \\
 0 & 0 & \mathbf{D}_s
 \end{bmatrix} \tag{12}$$

It can be observed that for symmetric laminate the submatrix  $\mathbf{D}_c$  vanishes indicating that there will not be any coupling between membrane and bending stress resultants. The elements of the stiffness matrix can readily be computed using the standard relation

$$K_{ij}^e = \int_{-1}^{+1} \int_{-1}^{+1} \mathbf{B}_i^T \mathbf{D} \mathbf{B}_j |J| d\epsilon d\eta \quad (13)$$

The computation of element stiffness matrix is economized by explicit multiplication of the  $\mathbf{B}_i$ ,  $\mathbf{D}$  and  $\mathbf{B}_j$  matrices instead of carrying out the full matrix multiplication of the triple product. Due to symmetry of the stiffness matrix, only blocks lying on one side of the main diagonal are formed.<sup>23</sup>

The consistent load vector  $\mathbf{P}$  due to distributed load  $p(t)$  is given by

$$\mathbf{P}(t) = \int_{-1}^{+1} \int_{-1}^{+1} \mathbf{N}^T p(t) |J| d\epsilon d\eta \quad (14)$$

In the present theory the loads may or may not act on the reference plane. The loads  $p_z^+(t)$  and  $p_z^-(t)$  are assumed to act on the positive and negative extreme  $z$  planes respectively. When transformed in the context of the present theory, the consistent load vector  $P(t)$  given by eqn (14) becomes,

$$\mathbf{P}(t) = \sum_{p=1}^m \sum_{q=1}^m W_p W_q |J| \mathbf{N}_i \left\{ \begin{array}{c} 0 \\ 0 \\ 1 \\ 0 \\ 0 \\ h/2 \\ 0 \\ 0 \\ h^2/4 \\ 0 \\ 0 \end{array} \right\} [p_z^+(t) + p_z^-(t)] \quad (15)$$

where  $h$  is the total thickness of the plate,  $W_p$  and  $W_q$  are the weighting coefficients,  $m$  is the numerical quadrature points in each direction and  $J$  is the standard Jacobian matrix.



2. The total mass of the element,

$$M^e = \int_V \rho dV = \int_A \rho t dA \quad \text{is also computed.}$$

3. A number  $S$ , by adding the diagonal coefficients  $M_{ii}$  associated with translation (but not rotation) is formed.
4. The diagonal coefficients of the mass matrix,  $M_{ii}$  are scaled by multiplying them by the ratio  $M^e/S$ , thus preserving the total mass of the element.

After the mass matrix is diagonalized, eqn (18) can be written as

$$\mathbf{a}_i^{n+1} = [(\Delta T)^2/M_{ii}] \left\{ - \sum_{j=1}^{NE} \mathbf{K}_{ij} \mathbf{a}_j^n + \mathbf{P}_i^n \right\} - \mathbf{a}_i^{n-1} + 2\mathbf{a}_i^n \quad (19)$$

If the values of  $\mathbf{a}^0$  and  $\dot{\mathbf{a}}^0$  are prescribed as initial conditions, a special starting algorithm can be written by noting that

$$\dot{\mathbf{a}}^0 = (\mathbf{a}^1 - \mathbf{a}^{-1})/2\Delta T \quad (20)$$

and eliminating  $\mathbf{a}^{-1}$  from eqn (19) leads to the expression

$$\mathbf{a}_i^{n+1} = \left( \frac{\Delta T^2}{2M_{ii}} \right) \left( - \sum_{j=1}^{NE} \mathbf{K}_{ij} \mathbf{a}_j^n + \mathbf{P}_i^n \right) + \mathbf{a}_i^n + \dot{\mathbf{a}}_i^n \Delta T \quad (21)$$

The estimate of critical time step is crucial in transient analysis because the use of time step more than the critical will lead to numerical instability.

The following estimates due to Leech,<sup>21</sup> Tsui and Tong<sup>22</sup> and Hinton<sup>16</sup> respectively were used as a guide:

$$\Delta T_1 \leq 0.25(\rho h/D)^{1/2}(\Delta x)^2 \quad (22)$$

$$\Delta T_2 \leq \Delta x \left[ \frac{\rho(1-\nu^2)/E}{2+0.83(1-\nu)\{1+1.5(\Delta x/h)^2\}} \right]^{1/2} \quad (23)$$

$$\Delta T_3 \leq \gamma \Delta x \left[ \frac{\rho(1-\nu^2)/E}{2+0.83(1-\nu)\{1+1.5(\Delta x/h)^2\}} \right]^{1/2} \quad (24)$$

where  $D = Eh^3/12(1-\nu^2)$ ,  $\Delta x$  is the minimum distance between finite element node points and  $\gamma$  is the correction factor, equal to unity for quadratic Lagrangian elements.

#### 4 NUMERICAL EXAMPLES AND DISCUSSION

The transient response has been studied by using 4-, 8- and 9-noded isoparametric elements. The selective integration scheme is used throughout the study, i.e. the  $3 \times 3$  Gauss rule is used to integrate the membrane, bending and inertia terms and the  $2 \times 2$  Gauss rule was used to integrate the shear terms numerically. All arithmetical calculations were performed in single precision on a CDC CYBER 180/840 machine.

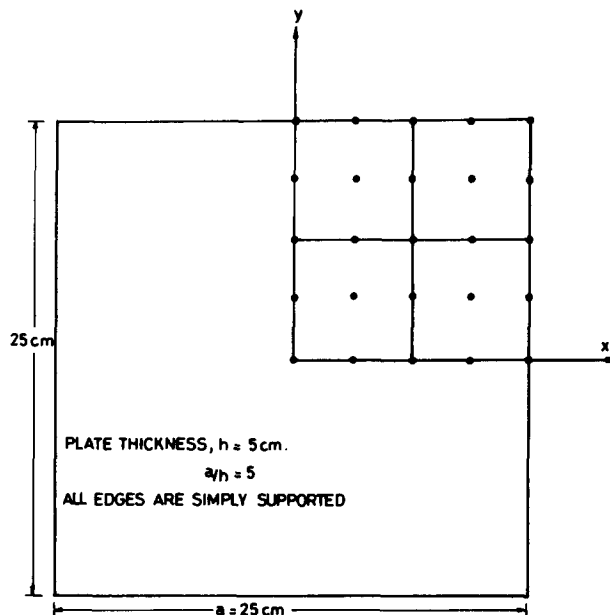


**Fig. 3.** Geometry boundary conditions and finite element mesh for the square plate problem.

In the present study numerical examples drawn from literature<sup>20</sup> are considered for establishing the reliability of our higher-order space-time discretization. As pointed out earlier we have simultaneously developed software based on the Mindlin<sup>24</sup> formulation and with exactly the same discretization procedure. This is done specially to cross check our results with a view to having confidence in our new formulation. A square plate with simply supported boundary conditions as shown in Fig. 3 is analysed throughout. Initial conditions of zero displacements and zero velocity are assumed throughout the plate in all the examples. Only one quarter of the plate is considered due to symmetry. A  $2 \times 2$  mesh of 9-noded Lagrangian isoparametric element is employed. All the stress values are reported at the

Gauss points nearest to their maximum value locations. The material properties considered for all numerical examples are as follows:

Whenever an isotropic plate is considered

$$E_1 = E_2 = E_3 = 2.1 \times 10^6 \text{ N/cm}^2 \quad (25)$$

$$\nu_{12} = \nu_{13} = \nu_{23} = 0.25$$

and whenever an orthotropic or layered plate is considered

$$\frac{E_1}{E_2} = \frac{E_1}{E_3} = 25, G_{12} = G_{23} = G_{13} = 0.5E_2$$

$$E_2 = 2.1 \times 10^6 \text{ N/cm}^2, \nu_{12} = \nu_{23} = \nu_{13} = 0.25 \quad (26)$$

**TABLE 1**

Convergence of Central Deflection ( $w \times 10^3$  cm) and Bending Stress with Different Time Steps for a Simply Supported Square Isotropic Plate Subjected to Suddenly Applied Uniform Load of  $10 \text{ N/cm}^2$  ( $a = 25 \text{ cm}$ ,  $h = 5 \text{ cm}$ ,  $E = 2.1 \times 10^6 \text{ N/cm}^2$ ,  $\rho = 8 \times 10^{-6} \text{ Nsec}^2/\text{cm}^4$ )

Time step ( $\mu\text{s}$ )	Mesh size	Time ( $\mu\text{s}$ )					
		40	80	120	160	200	
2	$2 \times 2$	$w$	0.217 9	0.951 1	1.473	1.669	1.175
		$\sigma_x$	7.68	90.56	123.9	156.0	96.3
	$3 \times 3$	$w$	0.214 5	0.950 7	1.470	1.663	1.168
		$\sigma_x$	4.305	88.65	119.3	153.9	97.28
	$4 \times 4$	$w$			Unstable		
		$\sigma_x$			Unstable		
1	$2 \times 2$	$w$	0.218 0	0.951 4	1.474	1.669	1.176
		$\sigma_x$	11.65	99.0	129.8	155.3	96.2
	$3 \times 3$	$w$	0.214 7	0.952 1	1.473	1.665	1.168
		$\sigma_x$	7.538	99.49	131.3	154.5	95.37
	$4 \times 4$	$w$	0.214 2	0.950 2	1.471	1.662	1.170
		$\sigma_x$	6.275	96.25	126.5	152.3	97.64
0.5	$2 \times 2$	$w$	0.218 0	0.951 4	1.473	1.669	1.176
		$\sigma_x$	12.37	98.34	125.5	156.4	102.2
	$3 \times 3$	$w$	0.214 8	0.952 1	1.472	1.664	1.169
		$\sigma_x$	8.477	99.05	125.0	151.5	101.2
	$4 \times 4$	$w$	0.214 2	0.950 2	1.471	1.662	1.170
		$\sigma_x$	7.009	96.23	124.7	155.2	103.9
0.25	$2 \times 2$	$w$	0.218 0	0.951 4	1.473	1.669	1.176
		$\sigma_x$	12.53	98.02	124.7	157.5	103.6
	$3 \times 3$	$w$	0.214 8	0.952 1	1.472	1.663	1.169
		$\sigma_x$	8.70	98.76	123.5	151.5	102.1
	$4 \times 4$	$w$	0.214 2	0.950 3	1.471	1.662	1.170
		$\sigma_x$	7.230	96.04	124.3	—	—

The numerical convergence and accuracy of the transient behaviour of the element are investigated through a simply supported isotropic plate with a suddenly applied uniformly distributed load of  $10 \text{ N/cm}^2$ . The results are given in Table 1.

Though the displacements seem to converge at  $\Delta T = 1 \mu\text{s}$ , the stress ( $\sigma_x$ ) converges at only  $\Delta T = 0.25 \mu\text{s}$ . Since the main aim of the study is to compare the performance of the higher-order plate element in transient analysis situations  $\Delta T = 0.25 \mu\text{s}$  is used with a  $2 \times 2$  mesh layout throughout.

#### 4.1 Example 1

An isotropic square plate subjected to a suddenly applied uniformly distributed load of  $10 \text{ N/cm}^2$  is considered. Table 2 gives the centre deflection and the bending stress ( $\sigma_x$ ) up to  $400 \mu\text{s}$ , using both Mindlin and

**TABLE 2**  
Central Deflection and Bending Stress for a Simply Supported Square Isotropic Plate Subjected to a Suddenly Applied Uniformly Distributed Load of  $10 \text{ N/cm}^2$

Time ( $\mu\text{s}$ )	<i>Present</i>					
	<i>Mindlin theory</i> <sup>20</sup>		<i>Mindlin theory</i>		<i>Higher-order theory</i>	
	$w \times 10^3$ (cm)	$\sigma_x$ (N/cm <sup>2</sup> )	$w \times 10^3$ (cm)	$\sigma_x$ (N/cm <sup>2</sup> )	$w \times 10^3$ (cm)	$\sigma_x$ (N/cm <sup>2</sup> )
20	0.039 9	0.126 3	0.049 6	0.949 2	0.049 5	0.243 9
40	0.185 5	6.533	0.219 1	4.683	0.218 0	12.530
60	0.533 9	44.15	0.583 6	48.88	0.569 3	53.02
80	0.924 9	82.77	0.974 3	91.57	0.951 4	98.02
100	1.227 8	103.9	1.278 4	111.6	1.254 0	113.1
120	1.459 1	120.2	1.502 4	124.8	1.473 0	124.7
140	1.653 7	144.4	1.692 3	154.9	1.659 0	147.8
160	1.666 7	149.5	1.694 2	157.2	1.669 0	157.5
180	1.460 4	124.2	1.496 4	132.1	1.478 0	135.4
200	1.172 8	94.96	1.180 4	96.74	1.176 0	103.6
220	0.866 9	74.30	0.880 2	78.93	0.876 6	85.22
240	0.541 0	49.22	0.544 7	50.37	0.549 8	58.59
260	0.171 1	5.291	0.199 8	10.48	0.212 3	13.89
280	-0.004 1	-8.085	-0.023 5	-15.59	-0.012 1	-15.81
300	0.000 9	0.241	-0.006 5	-2.03	-0.001 1	-3.385
320	0.104 5	7.046	0.107 1	7.676	0.098 3	1.273
340	0.295 8	17.47	0.301 0	18.55	0.281 6	23.25
360	0.629 5	48.49	0.609 8	43.69	0.583 1	46.13
380	—	—	1.033	92.70	0.983 1	93.42
400	—	—	1.370 2	125.1	1.326	121.80

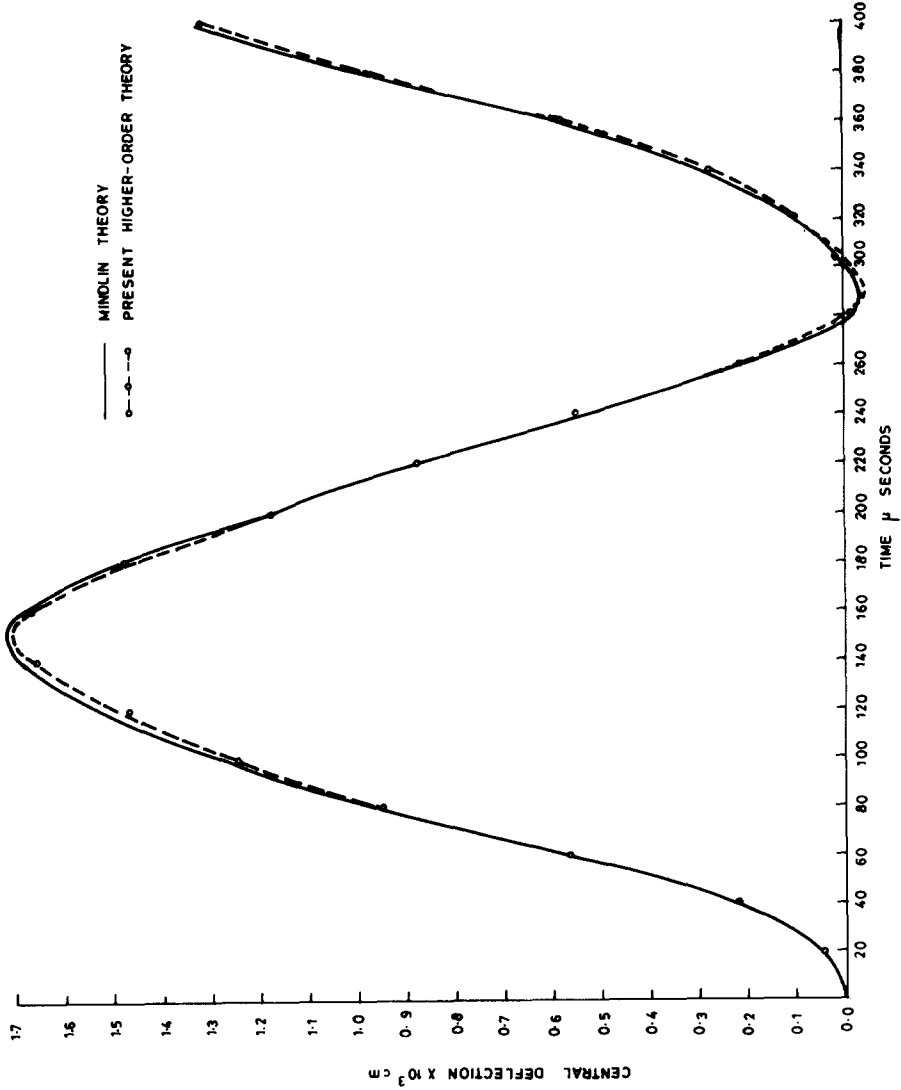


Fig. 4. Variation of central deflection with time.

**TABLE 3**  
Central Deflection and Bending Stress for a Square Orthotropic Plate Subjected to a Suddenly Applied Uniformly Distributed Load of  $10 \text{ N/cm}^2$

Time ( $\mu\text{s}$ )	Present					
	Mindlin theory <sup>20</sup>		Mindlin theory		Higher-order theory	
	$w \times 10^3$ (cm)	$\sigma_x$ (N/cm <sup>2</sup> )	$w \times 10^3$ (cm)	$\sigma_x$ (N/cm <sup>2</sup> )	$w \times 10^3$ (cm)	$\sigma_x$ (N/cm <sup>2</sup> )
20	0.039 8	24.64	0.050 4	30.77	0.050 5	39.92
40	0.193 9	132.2	0.224 6	155.2	0.224 1	197.5
60	0.430 3	282.1	0.455 1	312.2	0.444 1	399.7
80	0.553 1	359.3	0.560 7	380.4	0.548 3	471.1
100	0.526 4	349.7	0.515 8	355.2	0.501 6	461.8
120	0.370 5	345.4	0.340 1	232.7	0.327 4	272.8
140	0.177 9	115.1	0.155 8	103.8	0.150 8	128.5
160	0.035 3	22.00	0.018 8	12.31	0.012 3	20.09
180	-0.039 5	-20.97	-0.031 8	-24.52	-0.021 5	-24.77
200	0.110 5	73.61	0.141 2	95.62	0.142 4	119.5
220	0.329 6	214.1	0.354 2	242.6	0.351 4	294.5
240	0.478 1	316.8	0.503 2	342.5	0.501 8	441.3
260	0.554 8	368.9	0.550 9	379.8	0.532 8	501.0
280	0.479 7	314.5	0.454 0	307.3	0.434 6	365.1
300	0.200 6	194.9	0.269 2	183.9	0.258 2	229.5
320	0.084 0	59.38	0.057 4	39.7	0.043 3	34.22
340	-0.030 2	-18.53	-0.036 3	-28.8	-0.029 7	-13.14
360	0.045 9	28.57	0.064 6	43.37	0.072 0	51.85
380	—	—	0.233 3	157.3	0.252 0	198.2
400	—	—	0.408 9	281.4	0.405 0	389.2

the higher-order theory. Figure 4 shows the central deflection versus time plot.

#### 4.2 Example 2

A  $0^\circ$  orthotropic plate with the same loading as that of Example 1 is considered here. Table 3 gives the central deflection and bending stress ( $\sigma_x$ ) history for  $400 \mu\text{s}$ . The displacement response considering Mindlin as well as higher-order theory is presented in Fig. 5.

#### 4.3 Example 3

A 2-layered plate ( $0^\circ/90^\circ$ ) made of equally thick laminae subjected to a suddenly applied load whose spatial distribution is given by

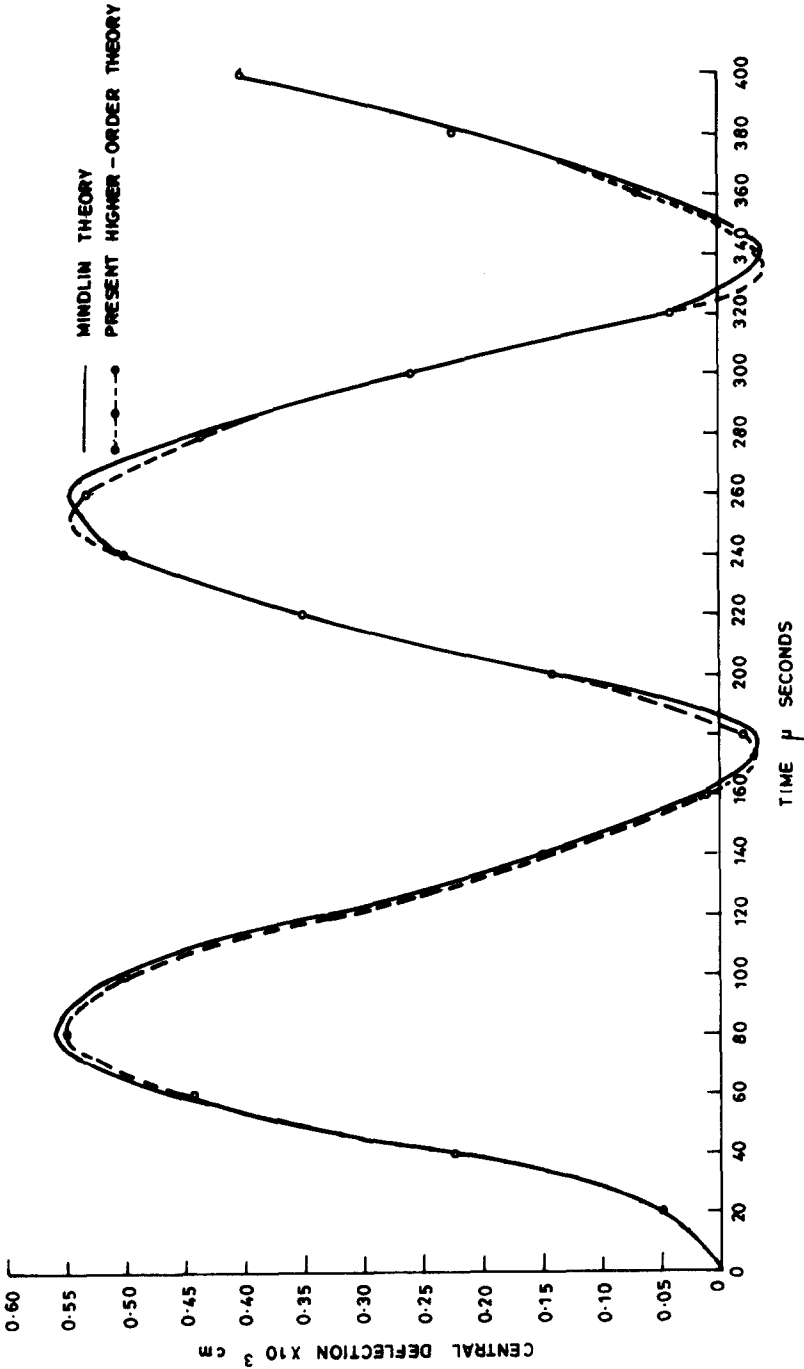


Fig. 5. Variation of central deflection with time.

**TABLE 4**  
Central Deflection and Bending Stress for a Simply Supported Square Cross-ply ( $0^\circ/90^\circ$ )  
Plate Subjected to a Suddenly Applied Sinusoidally Distributed Pulse Loading

Time ( $\mu\text{s}$ )	<i>Present</i>			
	<i>Mindlin theory</i>		<i>Higher-order theory</i>	
	$w \times 10^3$ (cm)	$\sigma_x$ (top) ( $\text{N}/\text{cm}^2$ )	$w \times 10^3$ (cm)	$\sigma_x$ (top) ( $\text{N}/\text{cm}^2$ )
20	0.046 4	36.84	0.046 0	41.85
40	0.165 4	127.8	0.162 9	131.1
60	0.310 8	242.7	0.307 5	236.3
80	0.423 8	333.1	0.421 2	305.4
100	0.460 0	363.3	0.463 9	349.3
120	0.405 8	321.4	0.415 2	316.5
140	0.281 2	220.3	0.295 8	228.9
160	0.137 6	106.3	0.151 2	111.0
180	0.029 5	20.13	0.038 9	34.60
200	0.002 4	1.48	0.001 5	13.63
220	0.065 8	52.35	0.052 7	48.33
240	0.195 0	154.0	0.174 3	83.52
260	0.338 5	265.8	0.317 9	232.3
280	0.438 4	342.8	0.429 5	330.7
300	0.456 5	359.0	0.462 2	347.7
320	0.384 0	302.3	0.407 8	304.5
340	0.251 9	199.7	0.283 8	211.8
360	0.110 2	86.11	0.141 4	117.7
380	0.016 9	11.23	0.032 0	36.14
400	0.008 4	4.11	0.002 2	4.402

$q(x, y) = q_0 \sin \pi x/a \sin \pi y/a$  is considered, where  $q_0 = 10 \text{ N}/\text{cm}^2$  and  $a = 25 \text{ cm}$  (side of the plate). The central deflection and the bending stress variation are summarized in Table 4 and Fig. 6.

#### 4.4 Example 4

A 2-layered plate ( $45^\circ/-45^\circ$ ) made up of equally thick laminae subjected to the same loading as in example 1 is considered. Table 5 shows the variation of maximum displacement and bending stress ( $\sigma_x$ ) over time. The above quantities are also plotted in Fig. 7.

From this figure, the effect of layers ( $45^\circ/-45^\circ$ ) and lamination angle on the amplitude and period of deflection is apparent. From Table 5 it is clear that Mindlin's theory predicts slightly lower values of deflection, period and

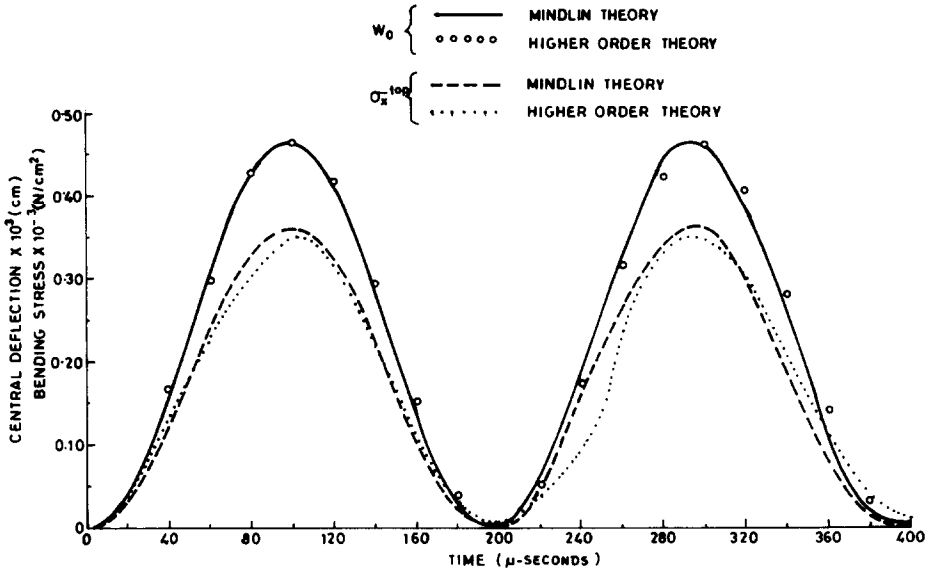


Fig. 6. Variation of central deflection and bending stress with time.

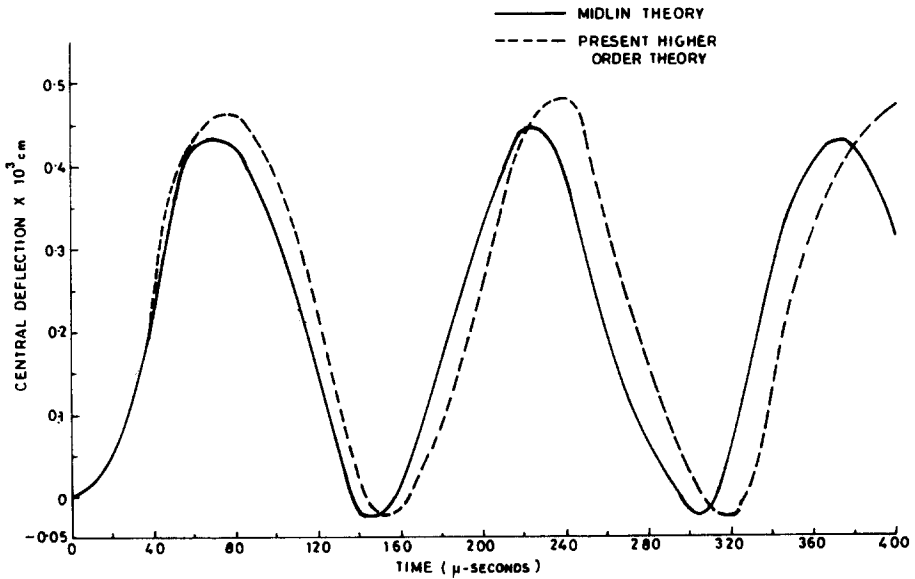


Fig. 7. Variation of central deflection with time.

**TABLE 5**  
 Central Deflection and Bending Stress for a Simply Supported Square Angle-ply  
 ( $45^\circ/-45^\circ$ ) Plate Subjected to a Suddenly Applied Uniformly Distributed Load of  
 $10 \text{ N/cm}^2$  (Full Plate is Discretized Here)

Time ( $\mu\text{s}$ )	<i>Present</i>			
	<i>Mindlin theory</i>		<i>Higher-order theory</i>	
	$w \times 10^3$ (cm)	$\sigma_x$ (bottom) ( $\text{N/cm}^2$ )	$w \times 10^3$ (cm)	$\sigma_x$ (bottom) ( $\text{N/cm}^2$ )
20	0.050 0	5.067	0.050 2	12.25
40	0.228 6	79.25	0.228 4	88.08
60	0.414 5	172.8	0.433 6	171.4
80	0.414 6	152.4	0.459 3	157.5
100	0.317 5	122.0	0.378 8	139.3
120	0.145 3	58.97	0.221 0	95.96
140	-0.020 7	-30.18	0.015 4	2.628
160	0.012 5	-1.650 5	-0.012 8	-15.93
180	0.166 6	67.52	0.103 7	36.24
200	0.315 8	107.0	0.257 0	90.07
220	0.449 0	184.2	0.442 0	171.2
240	0.384 8	151.8	0.480 3	185.1
260	0.192 1	56.82	0.332 2	108.0
280	0.061 5	28.98	0.173 1	76.97
300	-0.019 0	-21.91	0.022 6	18.29
320	0.062 8	6.259	-0.025 0	-28.41
340	0.281 4	120.7	0.130 7	42.99
360	0.396 4	146.6	0.321 8	120.9
380	0.416 0	159.4	0.432 7	162.1
400	0.316 4	132.9	0.473 8	186.4

stresses. The effect of transverse shear on the amplitude, period of the deflection and stresses is clear.

#### 4.5 Example 5

A 4-layered plate ( $30^\circ/45^\circ/90^\circ/0^\circ$ ) subjected to the same loading as in example 1 is analysed. This problem is solved specially to show that the higher-order theory gives a quadratic distribution of transverse shear stresses through the thickness, as shown in Fig. 8.

### 5 CONCLUSIONS

A higher-order shear flexible  $C^\circ$  plate bending element is developed and employed for the transient dynamic analysis of composite plates. Through

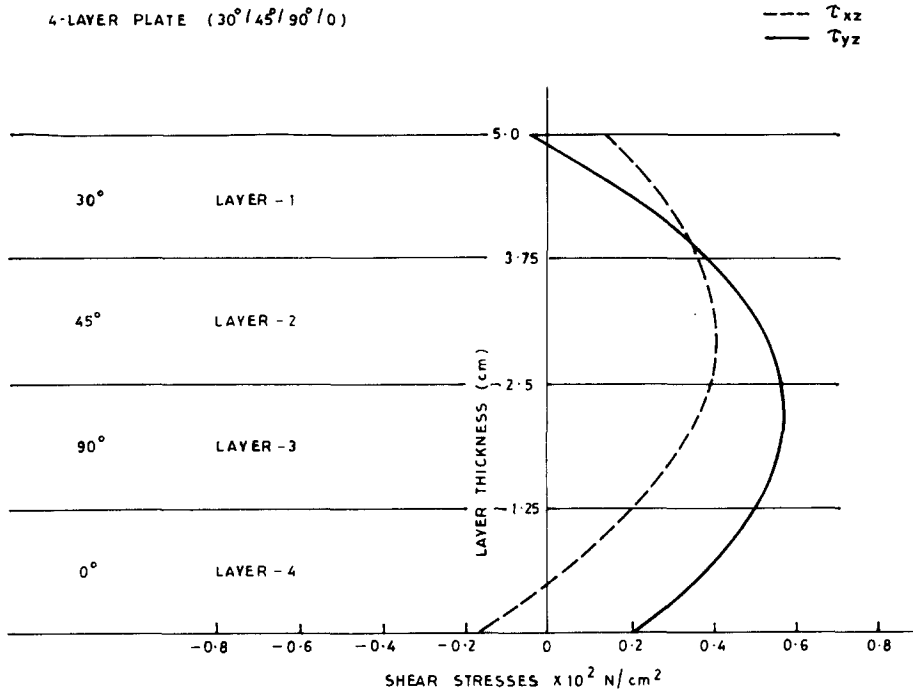


Fig. 8. Variation of transverse shear stresses over thickness (at time  $80 \mu\text{s}$ ).

the comparative studies done here, we clearly see the importance of this theory for highly anisotropic plates. The effects of neglecting shear deformation (as in classical lamination theory) and considering constant shear deformation (as in the first-order shear deformation Mindlin/Reissner theories) on the transient response of laminated composite plates are investigated. In contrast to the classical shear deformation theories, the present theory does not require a shear correction coefficient due to more realistic representation of cross-sectional deformation. In addition, the present theory includes the effect of normal stress ( $\sigma_z$ ) in the thickness direction which is, though negligible, very important in the study of delamination mode of failure in laminated composites.

The advantage in the use of the higher-order theory presented here over the Mindlin theory hitherto used is not quite evident for the isotropic plates. But such usage is very effective in the analysis of nonhomogeneous, anisotropic, composite or sandwich systems, and relatively thicker plates, as the mathematical model on which this theory is based is far superior to the Mindlin theory. It is, thus, seen that the formulation described here offers a convenient and concise method for the analysis of both thick and thin rectangular plates in bending.

## ACKNOWLEDGEMENT

Partial support of this research by the Aeronautics Research and Development Board, Ministry of Defence, Government of India, through its Grant No. Aero/RD-134/100/84-85/362 is gratefully acknowledged.

## REFERENCES

1. Calcote, L. R., *The analysis of laminated composite structures*, Van Nostrand Reinhold Co., New York, 1969.
2. Jones, R. M., *Mechanics of composite materials*, McGraw-Hill Ltd, New York, 1975.
3. Cook, R. D., *Concepts and applications of finite element analysis*, John Wiley and Sons, New York, 1981.
4. Reissner, E., The effect of transverse shear deformation on the bending of elastic plates, *ASME Journal of Applied Mechanics*, **12** (1945) A69–A77.
5. Mindlin, R. D., Influence of rotary inertia and shear deformation on flexural motions of isotropic elastic plates, *ASME Journal of Applied Mechanics*, **18** (1951) 31–8.
6. Murthy, M. V. V., *An improved transverse shear deformation theory for laminated anisotropic plates*, NASA Technical Paper—1903, 1981.
7. Phan, N. D. and Reddy, J. N., Analysis of laminated composite plates using a higher-order shear deformation theory, *International Journal for Numerical Methods in Engineering*, **21** (1985) 2201–19.
8. Lo, K. H., Christensen, R. M. and Wu, E. M., A higher-order theory of plate deformation—Part 1: Homogeneous plates, *ASME Journal of Applied Mechanics*, **44** (1977) 663–8.
9. Lo, K. H., Christensen, R. M. and Wu, E. M., A higher-order theory of plate deformation—Part 2: Laminated plates, *ASME Journal of Applied Mechanics*, **44** (1977) 669–76.
10. Kant, T., Numerical analysis of thick plates, *Computer Methods in Applied Mechanics and Engineering*, **31** (1982) 1–18.
11. Kant, T., Owen, D. R. J. and Zienkiewicz, O. C., A refined higher-order  $C^0$  plate bending element, *Computers and Structures*, **15** (1982) 177–83.
12. Pandya, B. N. and Kant, T., A refined higher-order generally orthotropic  $C^0$  plate bending element, *Computers and Structures* (in press).
13. Reismann, H., Forced motion of elastic plates, *ASME Journal of Applied Mechanics*, **35** (1968) 510–15.
14. Lee, Y. and Reismann, H., Dynamics of rectangular plates, *International Journal of Engineering Science*, **7** (1969) 93–113.
15. Rock, T. and Hinton, E., Free vibration and transient response of thick and thin plates using the finite element method, *Earthquake Engineering and Structural Dynamics*, **3** (1974) 51–63.
16. Hinton, E., The dynamic transient analysis of axisymmetric circular plates by the finite element method, *Journal of Sound and Vibration*, **46**(4) (1976) 465–72.
17. Pica, A. and Hinton, E., Transient and pseudo transient analysis of Mindlin

- plates, *International Journal for Numerical Methods in Engineering*, **15** (1980) 189–208.
18. Pica, A. and Hinton, E., Further developments in transient and pseudo-transient analysis of Mindlin plates, *International Journal for Numerical Methods in Engineering*, **17** (1981) 1749–61.
  19. Reddy, J. N., On the solutions to forced motion of rectangular composite plates, *ASME Journal of Applied Mechanics*, **49** (1982) 403–8.
  20. Reddy, J. N., Dynamic (Transient) analysis of layered anisotropic composite material plates, *International Journal for Numerical Methods in Engineering*, **19** (1983) 237–55.
  21. Leech, J. W., Stability of finite difference equations for transient response of flat plates, *AIAA Journal*, **3**(9) (1965) 1772–3.
  22. Tsui, T. Y. and Tong, P., Stability of transient solution of moderately thick plates by finite difference methods, *AIAA Journal*, **9** (1971) 2062–3.
  23. Gupta, A. K. and Mohraz, A., A method of computing numerically integrated stiffness matrices, *International Journal for Numerical Methods in Engineering*, **5** (1972) 83–92.
  24. Kant, T. and Sahani, N. P., Fibre reinforced plates—some studies with 9-noded Lagrangian/Heterosis element, *Trans. 8th International Conference on Structural Mechanics in Reactor Technology (SMiRT-8)*, Paper B 8/7, 315–20, North Holland Publishing Company, The Netherlands.